REVISTA
INTERDISCIPLINAR DE
PESQUISA EM
ENGENHARIA

INFLUENCE OF THE DIFFERENTIAL STRESS AND THE ORGANIC PATCHES ON THE CRACK PROPAGATION IN SHALES BY A DEM-FV SIMULATION

Marcello Goulart Teixeira

marcellogt@dcc.ufrj.br

Computer Science Departament, Federal University of Rio de Janeiro, Brazil

Frederic-Victor Donzé

Efthymios Papachristos

frederic.donze@3sr-grenoble.fr

efthymios.papachristos@3sr-grenoble.fr

Univ. Grenoble Alpes & CNRS, 3SR, CS 40700, F-38058, Grenoble cedex 9, France

François Renard

francois.renard@univ-grenoble- alpes.fr

Departments of Geosciences and Physics, Physics of Geological Processes, University of Oslo, Norway

Univ. Grenoble Alpes & CNRS, ISTerre, CS 40700, F-38058, Grenoble cedex 9, France

Hamed Panahi

hamed.panahi@gmail.com

Univ. Grenoble Alpes & CNRS, ISTerre, CS 40700, F-38058, Grenoble cedex 9, France

Luc Scholtés

luc.scholtes@univ-lorraine.fr

Univ. de Lorraine & CNRS & CREGU, Laboratoire GeoRessources, Nancy, France

Abstract. *The coupling between chemical reactions and deformation in rocks can induce permanent damage and cracking that facilitate the circulation of fluids at large scale. This*

coupling process has been observed in various geological systems as weathering and erosion of rocks on the surface, hydration of the lower crust, sediment dehydration in subduction zones, serpentinization of oceanic crust or sediment rock. Among the sedimentary rocks, shale has gained prominence due to growing unconventional exploitation of gas and oil. In this geological material, the coupling between organic matter maturation and the creation of micro-crack connectivity is one of the mechanisms proposed to explain the primary migration of hydrocarbons. The aim of this work is to study the influence of the differential stress and the density of organic patches on the crack propagation in shales. To this end, the hydro-mechanical version of the open source Discrete Element Method (DEM) code YADE is used to simulate the organic material dilatancy-induced cracking. It is presented some numerical simulations of crack propagation and an analysis of the influence studied.

Keywords: *Shale fracturing, Discrete element method, Finite volume method*

1 INTRODUCTION

The coupling between chemical reactions and deformation in rocks can induce permanent damage and cracking that facilitate the circulation of fluids at large scale. This coupling process has been observed in various geological systems as weathering and erosion of rocks on the surface, hydration of the lower crust, sediment dehydration in subduction zones, serpentinization of oceanic crust or sediment rock. Among the sedimentary rocks, shale has gained prominence due to growing unconventional exploitation of gas and oil. In this geological material, the coupling between organic matter maturation and the creation of micro-crack connectivity is one of the mechanisms proposed to explain the primary migration of hydrocarbons.

Some recent works have talked about the hydro-fracturing in rocks by a DEM-FV approach. Chen and Drumm (2011) presented a one dimension solution to particle-fluid coupled problems modeled by solving the averaged Navier–Stokes equation using the FVM and the solid phase modeled using the DEM. Catalano et all (2011) presented a model for fluid-saturated granular media coupled flow and mechanical deformation. Chareyre et all (2011) a coupled model for viscous fluid. Teixeira et al., (2016) shows that the state of stress in shales during maturation and the initial geometry of the kerogen patches control the final geometry of the microcracks produced

The aim of this work is to study the influence of the differential stress and the density of organic patches on the crack propagation in shales, giving an estimate to the P_{32} value depending on the vertical compress stress. To this end, the hydro-mechanical version of the open source Discrete Element Method (DEM) code YADE is used to simulate the organic material dilatancy-induced cracking. It is presented some numerical simulations of crack propagation and an analysis of the influence studied.

2 SIMULATION OF SHALE MATURATION

The shale fracturing under the action of maturation of the organic material was investigated using the YADE Open DEM plataform (Kozicki and Donze 2008, 2009; Smilauer et al., 2010), where the solid phase is characterized by a sphere packing DEM model and the fluid flow is solved by a Pore scale Finite Volumes (PFV) algorithm (Catalano, 2011).

At each cycle of computation, once the positions of the spheres are updated, new contacts are detected and the volumetric variation of pores is computed. The contact law and the fluid problem resolution give the contact forces (Scholtes 2012) and the fluid forces (Chareyre et al.) to be applied to particles, and the Newton's second law is applied to determine the resulting acceleration, which is then time integrated to find the new position. This process is repeated until the simulation is finished.

We choose here to model a tight rock with petrophysics parameters similar to a shale located at 5 km depth (Sone and Zoback, 2013), and fluid viscosity and bulk modulus similar to that of water. Table 1 shows the values of the parameters used to model the problem (Abousleiman, 1991, Islam and Skalle, 2013, Zhang and Scherer, 2012, Amann-Hildenbrand et al., 2012, Teixeira et al. 2016).

Table 1. Physical and microstructural parameters used for the numerical simulations

Shale model		Shale model patches		Fluid	
Density	2500 kg/m^3	Normal stiffness	1.0E9 Pa/m	Bulk	2.2x10^{-9} Pa
Porosity	6%	Shear stiffness	1.0E9 Pa/m	Viscosity	1.0^{-3} Pa s
Young's modulus	26x10^9 Pa	Tensile strength	0 Pa	Flow rate	1.0^{-6} m^3/s
Poisson's ratio	0.25	Cohesion	0 Pa		
Friction angle	25 ^{o}	Friction angle	25^o		
Tensile strength	0.8x10^6 Pa	Dilatancy	15^o		
Permeability	10^{-23} m^2				

It is considered a 26,0mm cubic sample, modeled by a sphere packing with 10000 discrete elements (Fig. 1). A coordination number N = 10, appropriated to a soft rock, was used (Scholtes and Donzé, 2013). The system is isothermal and heat exchanges are not considered.

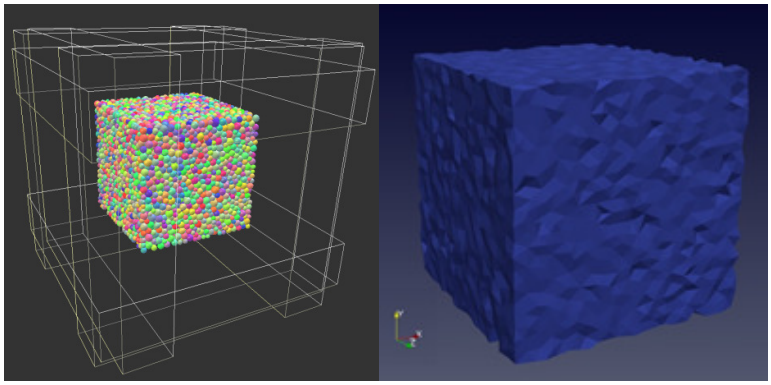

Figure 1: (a) spheres packing and (b) packing representation with faces

To simulate the kerogene maturation, the fluid is injected in the center of each joint in a constant flow rate. There is no boundary condition to the flow, so the fluid can go out the sample. It is simulated 0.006 s of fluid injection.

To understand the role of the compression stress, the quantity and relative location of joints on the fracturing, it was considered simulations with 1, 2 and 13 joints (Fig. 2 and Fig. 3). In each case, it was considered the flow rate equal to 10^{-6} m^3/s, the horizontal stresses $\sigma_h = \sigma_H$ = 80 MPa and different values of vertical compression stress (σ_y = 80, 90, 100 and 110 MPa).

In the simulations with 1 or 2 joints was considered the diameter of the joint equal to 6mm, but in this last one the joints are in different layers and the relative horizontal distance between them is equal to L = -2r, -r, 0, r and 2r, where r = 3mm and the minus represents the superposition of the joints.

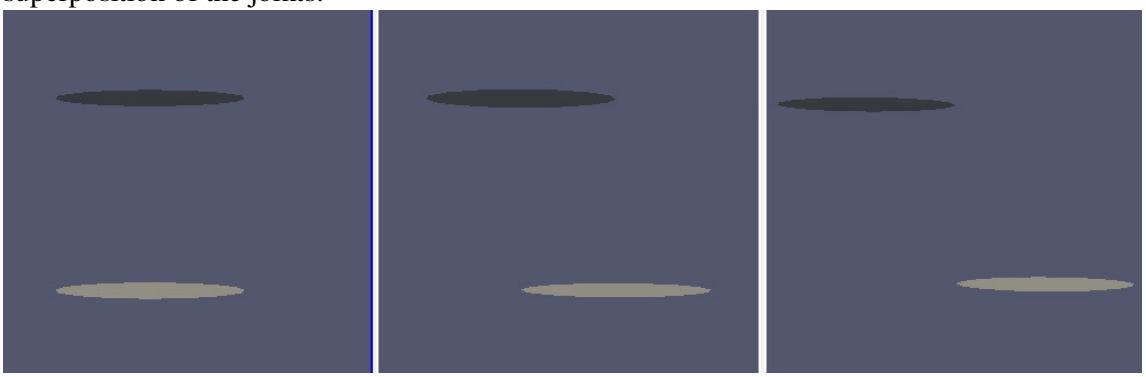

(a) (b) (c)

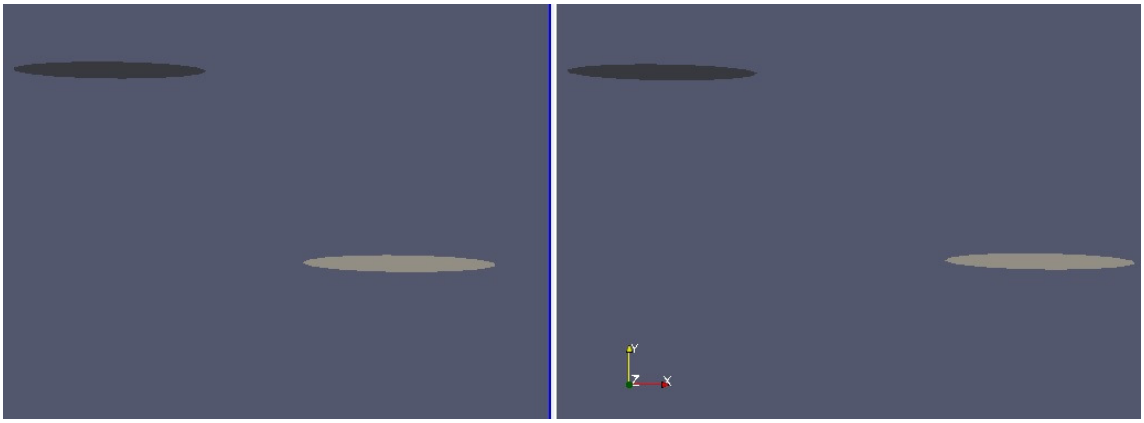

(d) (e)

Figura 2: Relative position of the two kerogenes zones: (a) $L = -2r$,(b) $L = -r$, (c) $L = 0$, (d) $L = r$, (e) $L = 2r$.

In the simulations with 13 joints they are in three different layers with 4, 5 and 4 joints, located respectively at 7, 13 and 19mm from the bottom. Their diameter d were considered equal to 5.8676mm, corresponding to a persistence p = 0.7071, where in this case the persistence is defined by $p = d / D$, with D the distance between the center of the joints. This value was chosen in such way that the total area of the joints in the intermediate layer is equal to 20% of the section area of the sample.

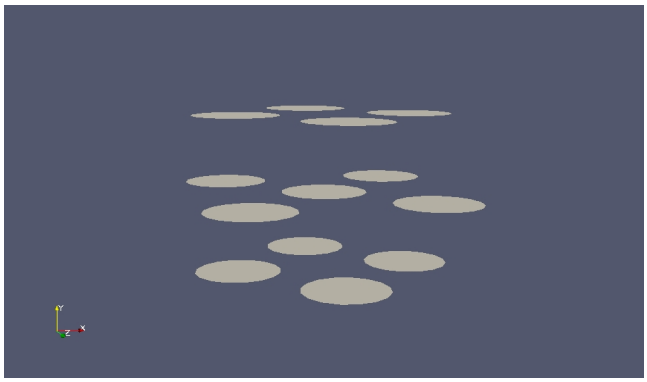

Figure 3: The 13 initial cracks.

To understand the formation of the micro cracks will be shown the P_{32} evaluation, where $P_{32} = \sum A_i / V$, with A_i the cross sectional area of the micro crack i, the C ratio evaluation, where $C = C_1 / C_2$, with C_1 the quantity of micro cracks located between two joint layers and C_2 the quantity of micro cracks close to the joints, and the normal vector angle θ of the micro crack with respect to the vertical axes (Fig 4). In all these cases are not considered microcracks whose center is at a distance equal to or less than 3 mm of the sample boundaries (fray area in Fig. 4a).

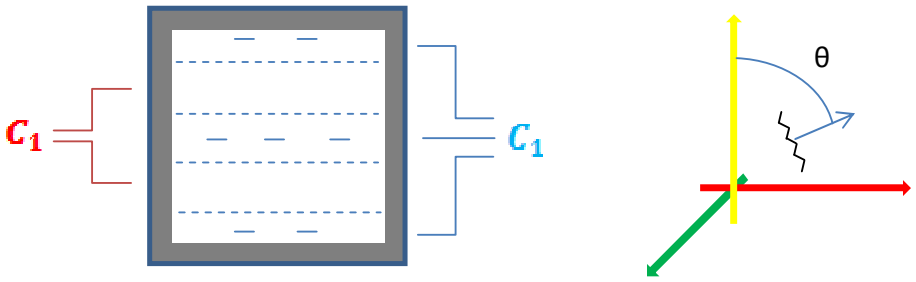

Figure 4: (a) C_1 and C_2 layers (side view of the sample) and (b) definition of θ

2.1 Single crack

In this case is considered a d = 6mm joint located at the center of the sample. The values of the vertical compress stress considered are σ_v = 80, 90, 100 and 110 MPa. In Fig. 5 is showed a zoom around the kerogen zone. The red discs represent the microcracks formed after the fluid injection and the black area represents the fluid. It is possible to see that the fluid flow changes under great values of vertical stress.

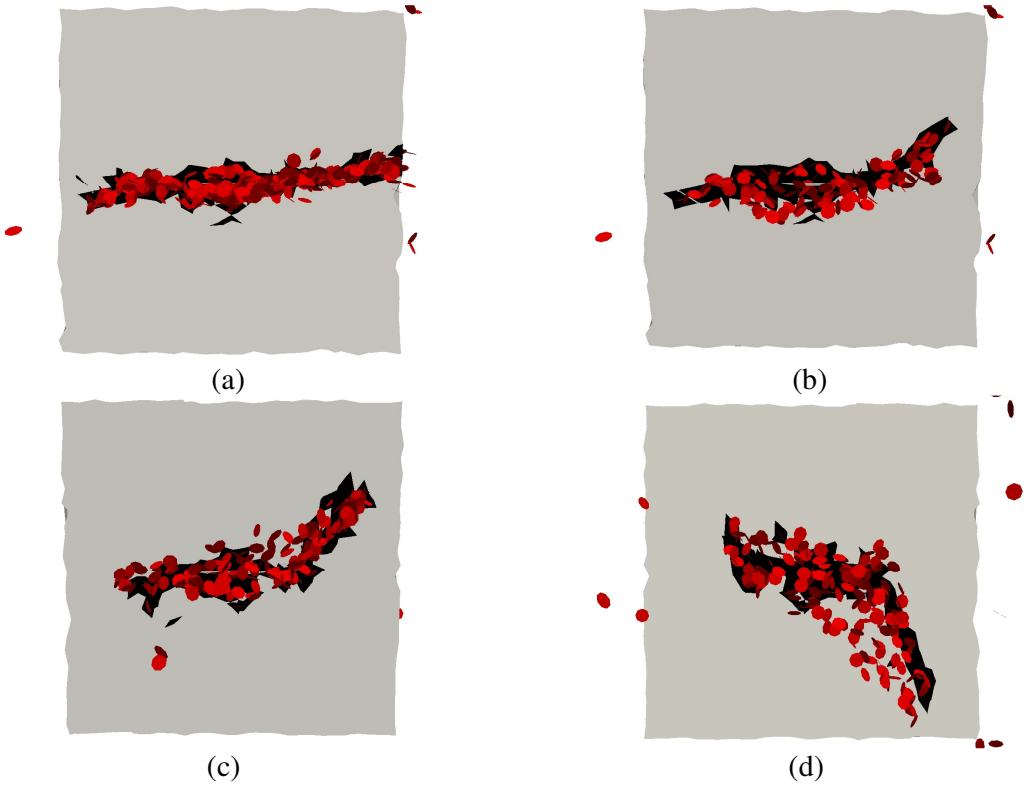

Figure 5: Microcracks (red discs) and fluid flow (black area) for (a) σ_v = 80 MPa, (b) σ_v = 90 MPa, (c) σ_v = 100 MPa and (d) σ_v = 110 MPa.

Figure 6 shows the quasi-linear growing of the P_{32} value. The difference between the greater (σ_v = 80MPa) and the lower (σ_v = 110MPa) value is around 17% at the end of the simulation.

Figure 7 presents the variation of *C* ratio and shows that the microcracks are formed mainly near of the initial crack and, as expected, this value is greater when the vertical compress stress is greater.

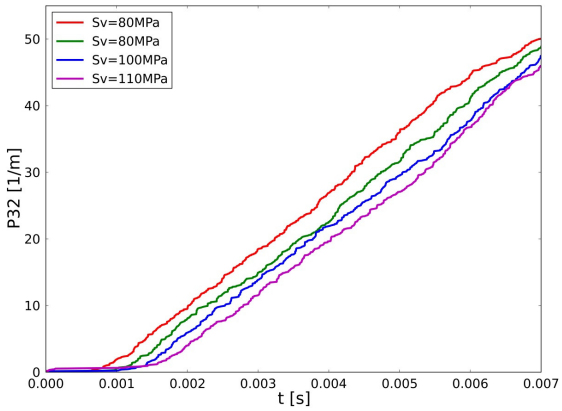

Figure 6: P_{32} evolution, one initial crak simulations.

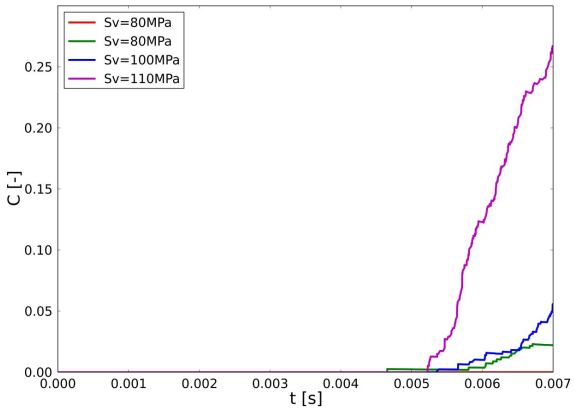

Figure 7: *C* ratio evolution, one initial crack simulations

One expected behavior, the gradual microcracks change of orientation with the growing of the vertical compress stress is showed in Fig. 8. Table 2 shows the mean value, the median and the standard deviation of the angle between the microcrak normal vector and the vertical axes.

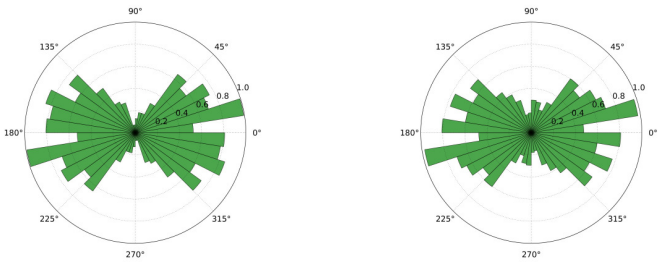

(a) (b)

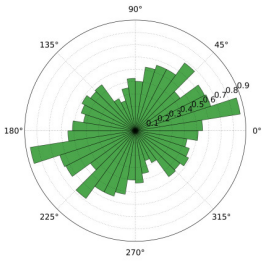

(c)

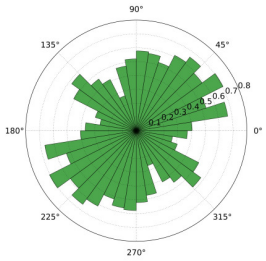

(d)

Figure 8: Normal vector angle of microcracks with respect to the vertical axes : (a) σ_v = 80MPa, (b) σ_v = 90MPa, (c) σ_v = 100MPa, (d) σ_v = 110MPa,

Table 2. Mean θ, median Θ and standard deviation *std* of the microcraks normal vector angle with respect to the vertical axes, $\sigma_h = \sigma_H$ = 80MPa.

Vertical compress stress	θ	Θ	std
80 MPa	47.35°	47.73°	18.41°
90 MPa	49.64°	49.36°	19.99°
100 MPa	54.77°	56.44°	21.16°
110 MPa	58.60°	60.39°	20.56°

2.2 Two cracks

With these simulations we were interested in to study the influence of the vertical compression stress and the horizontal relative distance between the kerogene zones, represented by the initial cracks. Figure 9 shows a zoom around the initial cracks, with σ_y = 80 MPa (left) and σ_y = 100 MPa (right), for L = -2r (a), L = 0 (b) and L=2r (c). The red discs are the microcracks formed after the fluid injection and the black area represents the fluid. It is possible to see that, under a greater value of the compress vertical stress, the fracturing between the layers is formed.

Figure 10 shows that the total area of the microcracks is greater when the vertical compress stress is greater, with the exception of the case L=-2r and σ_v = 100 MPa, where the P_{32} value at the end of the simulation is lower than in the hydrostatic case. This figure shows also that, in the hydrostatic case, the P_{32} value is greater when the initial cracks are closer or superposed, but this relationship is not preserved when σ_v = 100 MPa. This figure also shows a direct relation between the increase of the vertical compression stress and the decrease of the distance and the overlap of the initial fractures on the quantity of microcracks in the region between the initial cracks.

Figure 11 shows the orientation of the micro cracks at the last time step of the simulation and the Table 3 the values of mean, median and standard deviation of the normal vector angle of the microcracks. It is clear the influence of the vertical compress stress on the microcracks orientation but it is not possible to determine a direct relation between the superposition of the initial cracks and the normal vector angle.

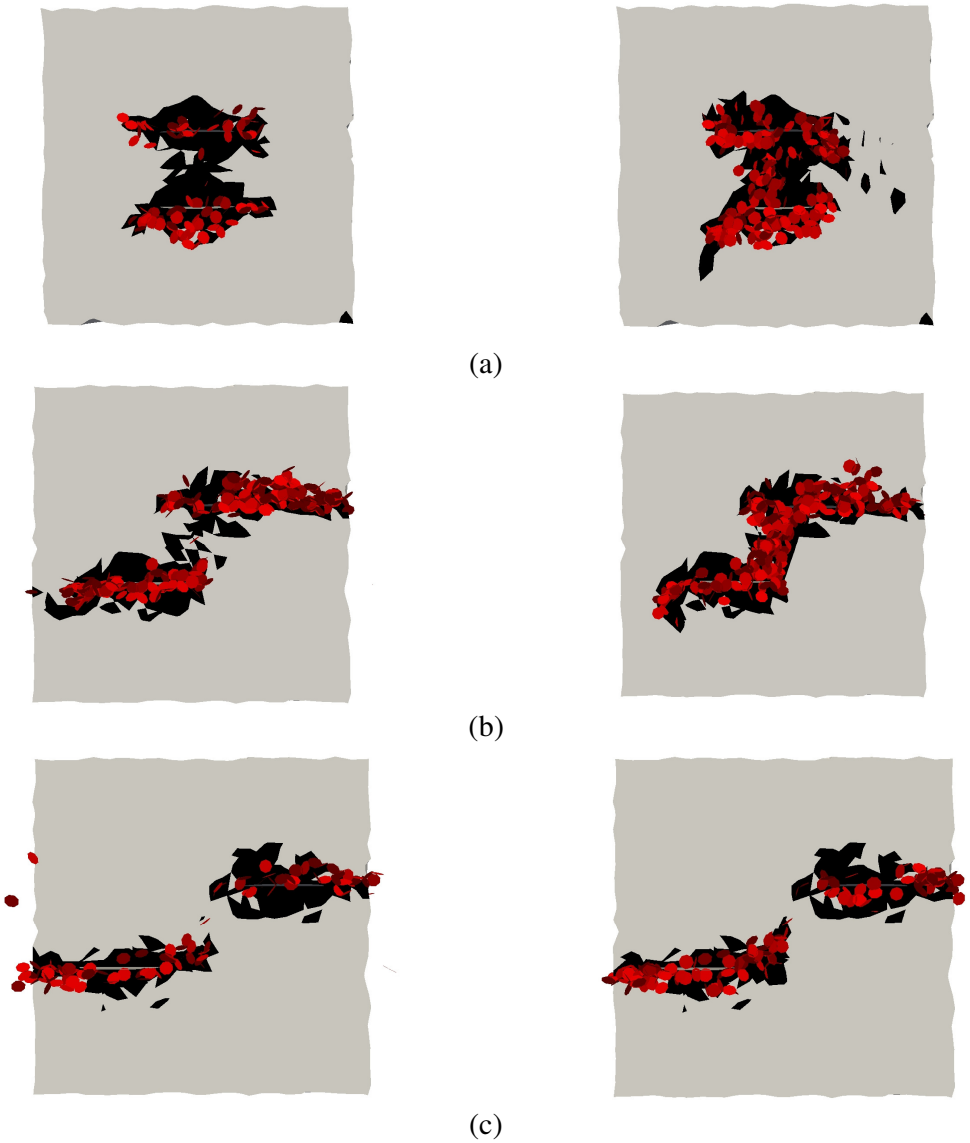

(a)

(b)

(c)

Figure 9: Microcracks (red discs) and fluid flow (black area) for the hydrostatic case (left) and σ_v = 100 MPa (right), with L = -2r (a), L = 0 (b) and L = 0 (c).

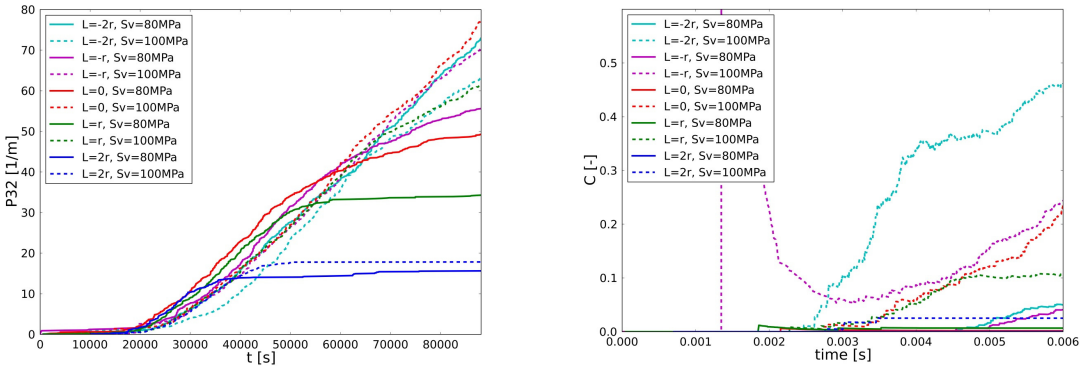

(a) (b)

Figure 10: P_{32} and C ratio evolution, two initial craks simularions.

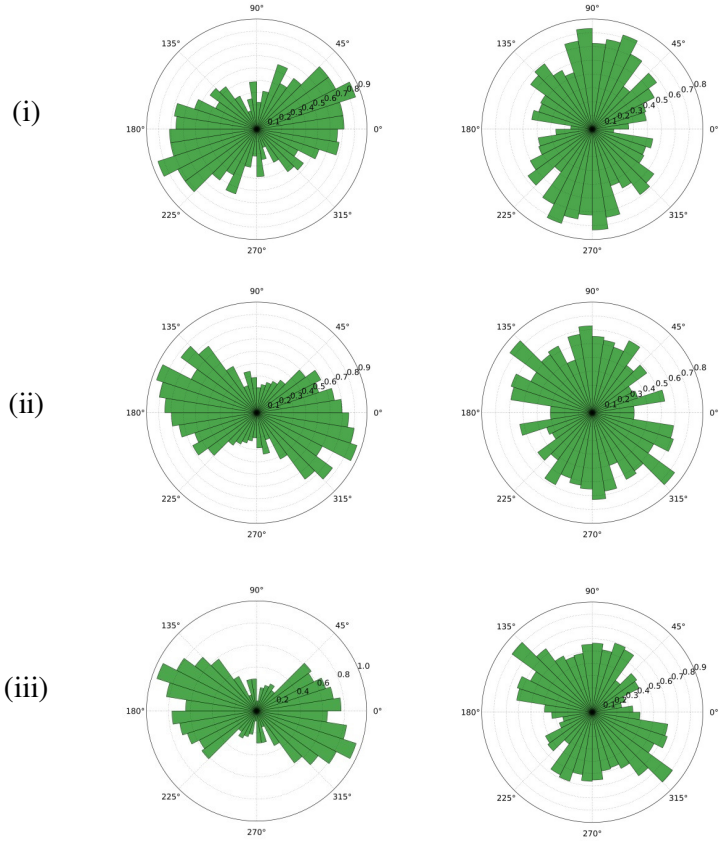

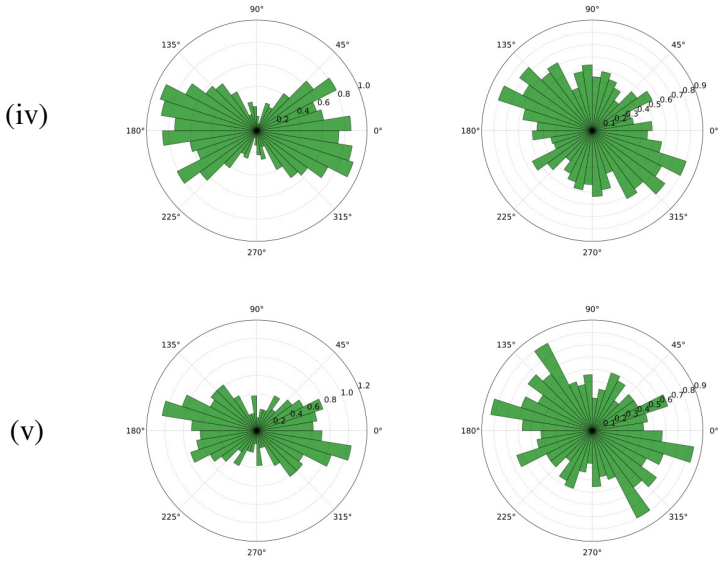

Figure 11: Normal vector angle of microcracks wit respect to vertical axes. (a) 80MPa, (b) 100MPa, (i) L = -2r, (ii) L = -r, (iii) L = 0, (iv) L = r, (v) L = 2r,

Table 3. Mean θ, median Θ and standard deviation *std* of the microcraks normal vector angle with respect to the vertical axes, $\sigma_h = \sigma_H = 80$MPa.

Vertical compress stress	80 MPa	100 MPa
L = -2r	$\theta = 50.93^o$ $\Theta = 50.85$ $std = 21.15^o$	$\theta = 62.33^o$ $\Theta = 65.71^o$ $std = 19.52^o$
L = -r	$\theta = 49.97^o$ $\Theta = 49.94^o$ $std = 20.74^o$	$\theta = 60.00^o$ $\Theta = 62.61^o$ $std = 20.46^o$
L = 0	$\theta = 48.24^o$ $\Theta = 48.13^o$ $std = 19.72^o$	$\theta = 59.55^o$ $\Theta = 61.74^o$ $std = 20.31^o$
L = r	$\theta = 49.97^o$ $\Theta = 49.94^o$ $std = 20.74^o$	$\theta = 60.00^o$ $\Theta = 62.61^o$ $std = 20.46^o$
L = 2r	$\theta = 49.06^o$ $\Theta = 48.57^o$ $std = 20.43^o$	$\theta = 55.37^o$ $\Theta = 56.31^o$ $std = 20.85^o$

2.3 Several cracks interacting

In the several cracks interacting examples there are 13 joints located at the points (a, 0.007m, b) and (a, 0.019m, b), where $a,\ b \in \{0.007\text{m}, 0.019\text{m}\}$, (0.013m, 0.013m, 0.013m) and (a, 0.013m), where $a,\ b \in \{0.013\text{m}, 0.019\text{m}\}$ (Fig. 3). The joints diameter is equal to

0.0058676, corresponding to a persistence p = 0.7071. It is considered the vertical compress stress equal to 80, 90, 100 and 110 MPa.

Figure 12 presents a vertical cut of the sample at t = 0.006s after the fluid injection with σ_y = 80 MPa in (a) and σ_y = 100 MPa in (b). The black zone represents the fluid and the red discs the microcracks formed after the fluid injection into the kerogen zones, represented by the gray discs. Below, the lines represent the principal stress σ_1 at the vertical section located at the domain center. It is possible to see in (a) that the fracturing is mainly horizontal, between the kerogene zones at the same layer, while in (b) there is also a fracturing between the different layers.

Figure 13(a) shows the P_{32} variation for the different values of vertical stress. The relation between the C ratio and the vertical stress is shown in Figure 13(b). The influence of the vertical compress stress on the microcracks normal vector angle with respect to the vertical axes can be seen in Fig. 14. It is possible to note that the compress stress changes the orientation of the cracks, as it was spected.

The Table 4 presents the mean values θ of normal vector angle of the microcracks, the C ratio and the P_{32} value for the values of compress vertical stress adopted.

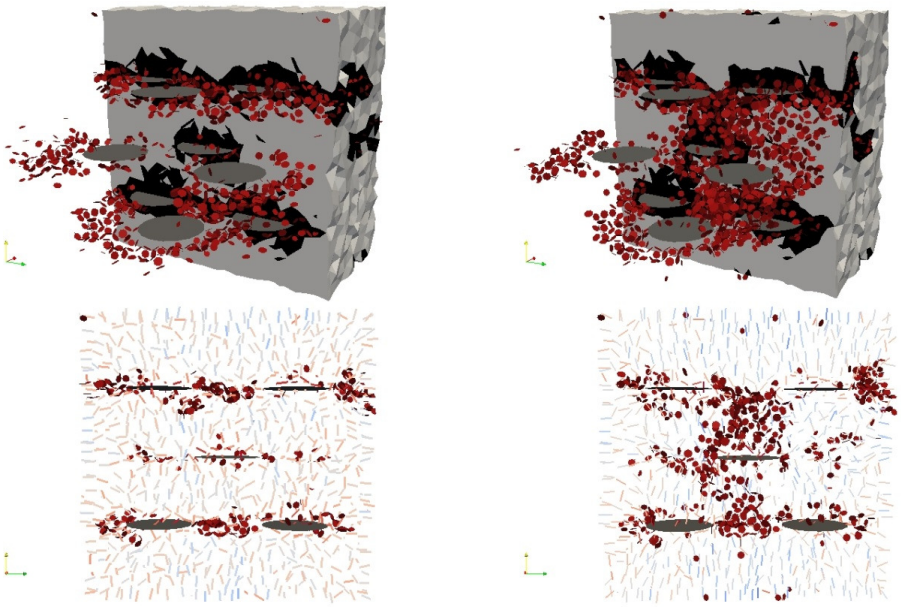

(a) (b)

Figure 12: Microcracks and fracturated cells (above) and microcracks and the principal stress σ_1 (below) for the hydrostatic case (a) and σ_v = 100 MPa (b)

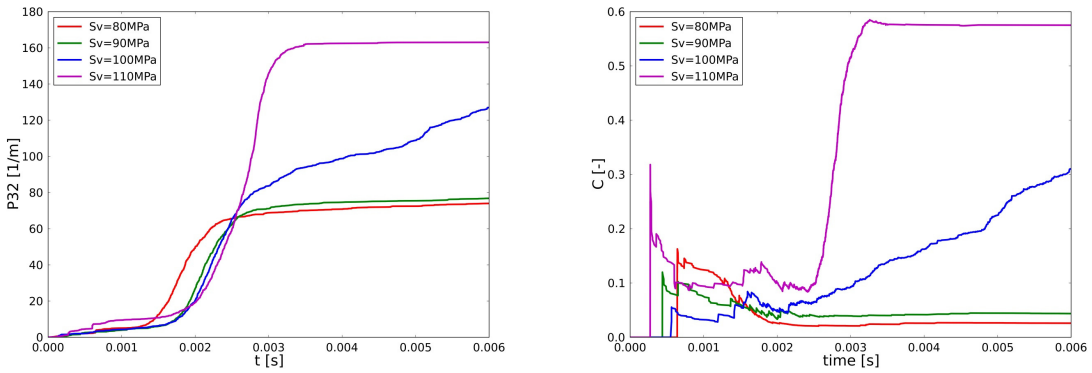

(a) (b)

Figure 13: P_{32} and C ratio variation, 13 initial cracks, persistence $p = 0.7071$.

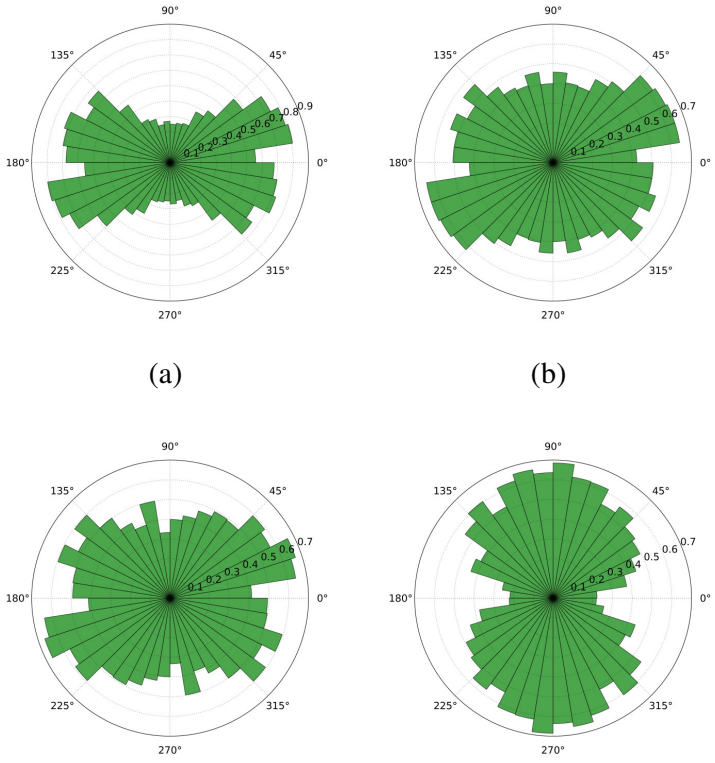

(a) (b)

(c) (d)

Figure 14: Normal vector angle of microcracks, 13 initial cracks simulations. (a) $\sigma_v = 80$ MPa, (b) $\sigma_v = 90$ MPa, (c) $\sigma_v = 100$ MPa and (d) $\sigma_v = 110$ MPa.

It is possible to note the quasi-linear relationship between the compress stress σ_v and the angle θ (Fig. 15). In fact, the linear fit $\theta(\sigma_v) = 0.4686\ \sigma_v + 12.818$ present a standard deviation

1.19952 and a correlation coeficient equal to 0.974459. The fit curves for C ratio and P32 are quadratic curves, given by $C(\sigma_v) = 0.0006\ \sigma_v^2 - 0.0952\ \sigma_v + 3.7605$, with $R^2 = 0{,}9837$, and $P_{32}(\sigma_v) = 0.0056\sigma_v^2 - 0.9568\sigma_v + 55.937$, with $R^2 = 0.9987$.

Table 4. Mean value of θ, C and P_{32}, with $\sigma_h = \sigma_H = 80$MPa.

Vertical compress stress	θ	C	P_{32}
80 MPa	50.00°	0.02675	15.3782
90 MPa	55.47°	0.04970	15.4645
100 MPa	55.41°	0.32448	16.4506
110 MPa	63.11°	0.58908	18.7872

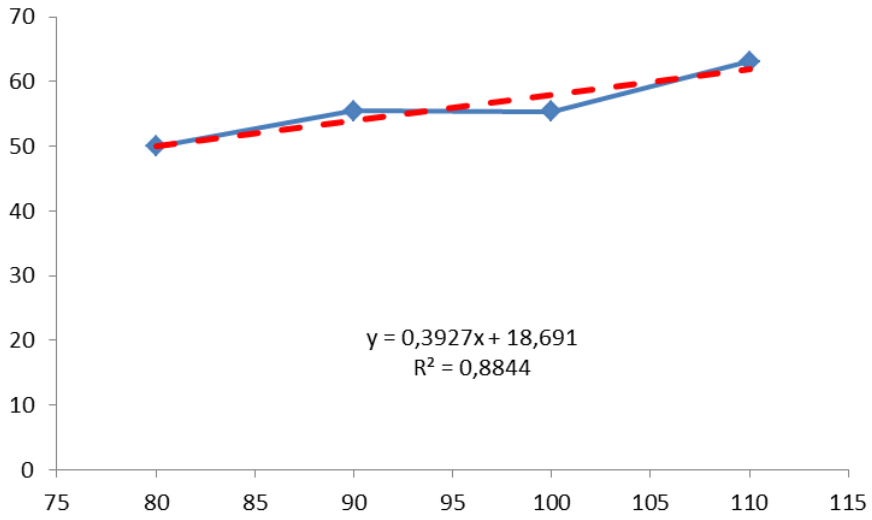

Figure 15: Angle variation and fit data

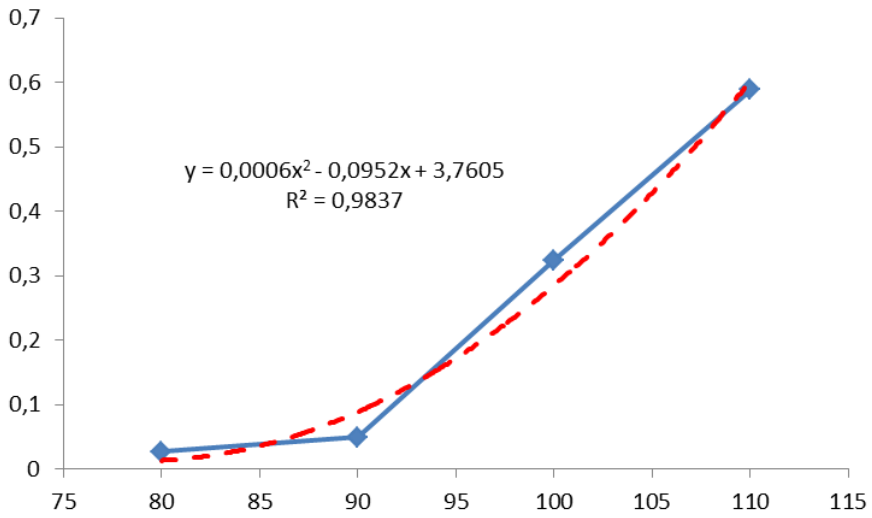

Figure 16: *C* ratio variation and fit data

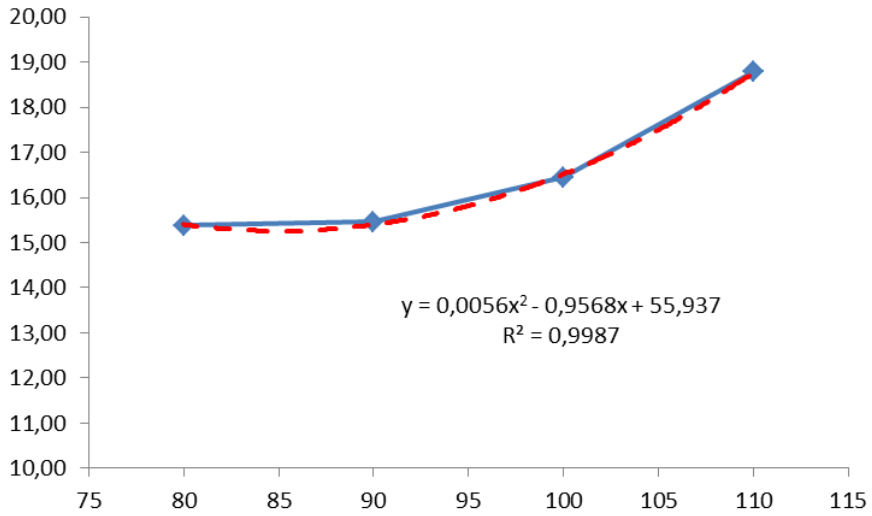

Figure 17: P_{32} ratio variation and fit data

3 DISCUSSIONS AND CONCLUSIONS

The shale fracturing under the action of maturation of the organic material was investing

The results for the theta are consistent, one time the mean and the median values are almost the same, and the standard deviation was around, but not greater then, 20o

The relationship between the vertical stress and the theta parameter is no-linear and a fit function was presented, giving good agreements to the estimatives extrapolada ou nao.

In the next steps of this research project will be studied the influence of the diameters and of the distance between the layers of the kerogen zones on the orientation and the number of microcracks.

ACKNOWLEDGEMENTS

The author MGT acknowledges the support from a research fellowship of CNPq.

REFERENCES

Abousleiman, Y.N. 1991. A Poroelastic PKN Model with Pressure Dependent Leakoff and Formation Permeability Determination, PhD dissertation, University of Delaware.

Amann-Hildenbrand, A., Ghanizadeh, A., Krooss, B. M., 2012. Transport properties of unconventional gas systems, *Marine and Petroleum Geology*, vol. 31, pp. 90-99.

Ben-Zion, Y., 2008. Collective Behavior of Earthquakes and Faults: Continuum-Discrete Transitions, Evolutionary Changes and Corresponding Dynamic Regimes. *Rev. Geophysics*, 46, RG4006, doi:10.1029/2008RG000260.

Ben-Zion, Y., K. Dahmen, V. Lyakhovsky, D. Ertas & A. Agnon, 1999. Self-Driven Mode Switching of Earthquake Activity on a Fault System. *Earth Planet. Sci. Lett.*, vol. 172, pp. 11-21.

Bos, B., Spiers, C.J., 2002. Fluid-assisted healing processes in gouge-bearing faults: insights from experiments on a rock analogue system. *Pure and Applied Geophysics*, vol 159, pp 2537-2566.

Catalano, E., Chareyre, B., Cortis, A., Barthelemy, E., 2011. A pore-scale hydro-mechanical coupled model for geomaterials. II International Conference on Particles-based Methods – Fundamentals and Applications.

Chareyre, B., Cortis, A., Catalano, E., Barthelemy, 2011. E. Pore-scale Modeling of Viscous Flow and Induced Forces in Dense Sphere Packings. (submitted) (2011)

Cundall PA, Strack ODL, 1979. A discrete numerical model for granular assemblies. *Geotechnique*, vol 29, pp 47–65.

Emanuele Catalano, Bruno Chareyre, Eric Barthélémy, 2014. Pore-scale modeling of fluid-particles interaction and emerging poromechanical effects. *Int. J. for Numerical and Analytical Methods in Geomechanics*, vol 38, n. 1, p. 51-71

Kozicki, J & Donze, F.-V., 2008. A new open-source software developed for numerical simulations using discrete modeling methods. *Comp. Meth. Appl. Mech. Eng.*, vol 197, pp. 4429–43.

Kozicki, J & Donze, F.-V., 2009. YADE-OPEN DEM. An open-source software using a discrete element method to simulate granular material. *Eng. Comput.*, vol 26, n 7, pp 786–805.

Islam, Ms. A., Skalle, P., 2013. An Experimental Investigation of Shale Mechanical Properties Through Drained and Undrained Test Mechanisms, *Rock Mech Rock Eng* vol. 46, pp. 1391–1413.

Scholtés, L., Donze, F.-V., 2012. A DEM model for soft and hard rocks: Role of grain interlocking on strength. *J. Mech. Phys*. Solids.

Scholtés, L. a, Donze, F.-V., 2012. Modelling progressive failure in fractured rock masses using a 3D discrete element method, *International Journal of Rock Mechanics & Mining Sciences*, vol 52, pp 18–30.

Sone, H., Zoback, M. D., 2013. Mechanical properties of shale-gas reservoir rocks – Part 1: Static and dynamic elastic properties and anisotropy, *Geophysics*, vol. 78, pp. D381-D392.

Teixeira, M. G., Donzé, F., Renard, F., panahi, H., Papachristos, E., Scholtè, L., Microfracturing during primary migration in shales, *Tectonophysics*, submeted in July 2016.

Zhang, J., Scherer, G. W., 2012. Permeability of shale by the beam-bending method, *International Journal of Rock Mechanics & Mining Sciences*, vol. 53, pp. 179–191.